Available online at www.sciencedirect.com
ScienceDirect
Polymer 48 (2007) 4075–4086
polymer
www.elsevier.com/locate/polymer

The effect of dispersion state on PMMA–epoxy–clay ternary blends: *In situ* study and final morphologies

M. Hernandez [a], B. Sixou [b], J. Duchet [a,*], H. Sautereau [a]

[a] *Laboratoire des Matériaux Macromoléculaires, UMR IMP CNRS #5627, INSA-Lyon, Bât. Jules Verne, 17 avenue Jean Capelle, F-69621 Villeurbanne, France*

[b] *Groupe d'Etudes de Métallurgie physique et de Physique des Matériaux, UMR CNRS #5510, INSA-Lyon, Bât. B. Pascal, 7 avenue Jean Capelle, F-69621 Villeurbanne, France*

Received 14 February 2007; received in revised form 3 May 2007; accepted 3 May 2007
Available online 13 May 2007

Abstract

Two PMMA–epoxy–clay ternary composites have been produced combining the polymerization induced phase separation phenomenon with two individual dispersion processing methods: a melt-blending and an ultrasonic-blending. Transmission electron microscopy (TEM) analysis shows that phase separation between PMMA and epoxy network was obtained in the form of spherical nodules in both processing methods. Organoclay particles were finely dispersed into thermosetting network and predominantly delaminated in ultrasonic-blending, whereas organoclays formed micrometer-sized aggregates in melt-blending. Wide-angle-X-ray (WAXS) studies reveal that exfoliation in the clay particles in three-phase composite was reached. Exfoliation state has been investigated using small angle X-ray scattering (SAXS) in cured systems and during curing reaction. For reacted systems, an exfoliation of platelets can occur through the de-aggregation of large agglomerates into smaller particles composed of a few platelets. For *in situ* SAXS studies, the distribution of the thicknesses of diffusing entities and the evolution of this distribution with reaction time were followed. This technique has shown also that movements at scale of nanometers of clay tactoids are possible even after the gel point.

Keywords: Thermoplastic-thermosetting blend; SAXS dispersion; Lamellar silicate nanocomposites

1. Introduction

Interactions between inorganic layered materials and organic substances have attracted increasing interest from both scientific and industrial perspectives [1,2]. Nanoclay filled polymer materials provide possibilities of improving many properties over polymeric materials [1]. Thermal and tensile properties as well as resistance to flammability and distortion temperature, reduction of the permeability to solvents [3] are some examples of improvements that have been reported since Toyota Central Research Laboratories fabricated the first hybrid polymer–clay composite [4] with an exfoliated clay structure (nylon-6-montmorillonite). It has been demonstrated that the incorporation of lamellar fillers could change both the stiffness and the fracture toughness of epoxy materials, the balance toughness/stiffness varying with the exfoliation extent [5–7]. One important and interesting fact is that the state of dispersion of the clay in the polymer governs many properties. Sodium montmorillonite (MMT) is one of the more popular clay used for developing polymer nanocomposites [8], it has the particularity of having different levels of organization according to the scale of observation (Fig. 1). A single platelet (or layer) corresponds to a planar repetition crystalline cells which is formed by an octahedral layer composed of aluminium or magnesium oxide and also by two tetrahedral layers made of silicon oxides. A tactoid or primary particle is thus formed by 5–10 single platelets held by electrostatic forces. Aggregates are formed by several primary particles without

* Corresponding author. Fax: +33 4 724385 27.
E-mail address: jannick.duchet@insa-lyon.fr (J. Duchet).

0032-3861/$ - see front matter © 2007 Elsevier Ltd. All rights reserved.
doi:10.1016/j.polymer.2007.05.013

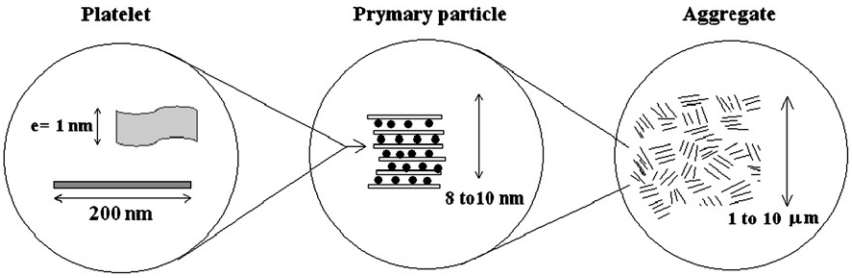

Fig. 1. Schematic representation of montmorillonite multiscale organization.

any specific orientation and this structure is more or less dense according to the texture, the number of particles and the distances between them [9]. To get a true nanocomposite, both aggregates and tactoids should be broken into their nanoscale building blocks with the help of some dispersion processes.

Generally three types of composite materials can be obtained when clay particles are dispersed in a polymeric matrix: (i) conventional composites containing clay tactoids in unintercalated face to face form; in this case the clay is dispersed simply as a segregated phase forming aggregates. (ii) Intercalated clay composites are obtained when one or a few polymer chains are placed into the clay host galleries. (iii) In exfoliated polymer–clay nanocomposites, the particles of the clay are dispersed individually into the matrix.

Traditionally, thermoplastics have been used for obtaining nanomaterials, however, many of these thermoplastics have a high viscosity causing some difficulties in the extrusion and injection moulding processes. Previously, some thermoplastics have been mixed with a low molecular weight plasticizer in order to lower the viscosity but this affects the polymer's mechanical properties. Thermosets in contrast are easily processed because they are obtained *in situ* from monomers. Among the thermosets, epoxies are widely used in many fields especially in the aeronautic industry as adhesives and in structural applications as matrices in composites [10] because of their high stiffness, and good heat and solvent resistance. Epoxy prepolymers are reactive monomers which are cured commonly with amines for obtaining thermosetting polymers. The thermosetting materials are limited because of their brittleness and over the last 30 years researchers have been trying to solve this problem by mixing the thermosetting resin with thermoplastics or elastomers in order to increase the toughness [11].

The thermoplastic initially miscible in the epoxy monomer undergoes a phase separation during the epoxy-hardener curing reaction because of the molar mass increase involving a decrease in the conformational entropy of mixing [10]. Polysulfone (PSu), poly(ether sulfone) (PES), polyetherimide (PEI), poly(ether ether ketone) (PEEK) and poly(methylmethacrylate) (PMMA) are the thermoplastic modifiers that have been the most frequently studied. Many researchers have focused on finding interactions in DGEBA–PMMA blends, but no specific interaction between PMMA and DGEBA has been detected even after heating the mixture for several hours. Ritzenthaler et al. [12] and Gomez and Bucknall [13], say that a complete miscibility of the polymer with the epoxy prepolymer before curing occurs, and that a phase separation is observed after curing. The morphology of the generated materials depends on the initial formulation (chemical nature of precursor, thermoplastic weight fraction, etc.) and curing conditions (reaction rate, viscosity, etc.).

The key objective in preparing polymer–clay nanocomposites is to achieve exfoliation or delamination of the aggregates into tactoids and then into single layers because the improvement in final properties of nanocomposites is highly dependent on the degree of clay dispersion [14]. But the final morphology often results from a coexistence of exfoliated sheets, tactoids and micron-size agglomerates.

Transmission electron microscopy (TEM) is the best usual method to obtain a direct visualization of the dispersion state. Few studies give a quantitative image analysis of TEM micrographs [15]. Moreover, TEM only probes a very small volume which may or may not be representative of the whole sample. Unlike TEM which is a local analytical technique, small angle X-ray scattering (SAXS) is a powerful technique for studying the structure of polymer systems since the analysed volume is about 1 mm^3 with standard equipment. This technique is sensitive to structural features on length scales of 1–100 nm [16–19]. Yet due to the experimental uncertainties at very small angles, only entities smaller than 50–100 nm can be observed by SAXS. In polymer–clay nanocomposites, SAXS can give interesting results concerning this distribution of the tactoid thicknesses [20].

The proportion of micron-size agglomerates is often neglected whereas it is necessary to characterize the dispersion of the montmorillonite (MMT) platelets from the nanometer scale to the micron scale. Some works have shown that the dispersion state of silicate layers might evolve during the network cross-linking when the competition between cure and diffusion kinetics and interactions between network precursors and organophilic montmorillonite allows it [21,22]. It was found that faster intragallery polymerization, catalysed by the organic modifier, produced exfoliated clay structures: the individual clay layers were pushed out of the tactoids by the gradual diffusion of epoxy polymer into the clay gallery. Park and Jana [11] have evoked other mechanisms than the disparity of rates between intra and extragallery polymerization to explain exfoliation phenomena in epoxy–nanoclay systems. Exfoliation goes on up to epoxy-amine gelification, provided that the ratio of storage modulus to complex viscosity

was kept above 2–4 s^{-1}, such that elastic forces inside the galleries outweigh the viscous forces offered by the extragallery epoxy.

In this work, we have studied the incorporation of both a thermoplastic and clay particles in an epoxy-amine system both to increase the toughness of epoxy thermosets and to improve silicate layer dispersion. Poly(methylmethacrylate) PMMA was chosen due to its solubility in the initial blend of diglycidyl ether of bisphenol A (DGEBA). The phase separation of epoxy–PMMA cured blends is strongly dependent on the curing agent used. Ritzenthaler et al. [12] have shown that using MDA hardener and 10 phr of PMMA, small nodules of PMMA inside the matrix were present. Yet, there are not many studies on the PMMA–montmorillonite–epoxy amine ternary systems [11]. In this paper, we want to understand how the ternary blend preparation will have an effect on the exfoliation state of the layers in the ternary nanocomposites. Two processing techniques have been used and compared for this study: one employing melt intercalation and the other using ultrasonic processing. In order to understand the exfoliation mechanisms in this ternary blend, we will follow the dispersion of platelets during the curing reaction and we will investigate the influence of the preparation method on the final morphologies obtained.

2. Experimental details

2.1. Materials

In this study the epoxy prepolymer used was the aromatic diglycidyl ether of bisphenol A (DGEBA) with an average number of hydroxyl groups per two epoxy groups of $\overline{n} = 0.15$ (LY556 from Vantico). The hardener was the aromatic 4,4′-methylene dianiline (MDA) with an analytical grade from Aldrich. The clay used was the montmorillonite (MMT) (Cloisite 30B) from Southern Clay Products, which was modified by methyl, tallow, and bis-2-hydroxyethyl quaternary ammonium chloride ions. The polymer employed was a PMMA with an average molar mass of 50,000 g mol^{-1}. Tetrahydrofuran (THF) was used as solvent. The different characteristics and structures of materials are listed in Table 1.

2.2. Processing

In the present work, samples were processed by using in one case a traditional melt dispersion tool and in the other case an ultrasonic dispersion tool.

2.2.1. Melt dispersion

DGEBA and PMMA are mixed in a glass reactor at 135 °C, after 2 h the solution becomes homogeneous and transparent the clay is then added and it is mixed with a Rayneri turbo mixer at 2000 rpm during 2 h, finally the curing agent is introduced into the system and the mixing is stopped after 5 min. The different steps are summarized in Fig. 2.

2.2.2. Ultrasonic probe dispersion

PMMA is dissolved in a THF solution at a concentration of 10 wt% helped by a magnetic stirring at 40 °C for 1 h, after that the clay is added and all the system is mixed using an ultrasonic probe at room temperature during 30 min. The solution and DGEBA are placed into a glass reactor and mixed mechanically using a Rayneri turbo at 2000 rpm at 135 °C for 2 h, finally the amine is added and the mixture is stopped after 5 min. The different steps are summarized in Fig. 3.

In both cases, the hardener is used at stoichiometric ratio of epoxy to amino-hydrogen groups equal to 1 and a loading of 10 phr and 5 phr of PMMA and Cloisite 30B (known as 30B) are employed, respectively. After the amine dissolution step at 135 °C, all the mixtures are submitted to a curing cycle including 4 h at 135 °C and 2 h at 200 °C into a metallic mold covered with PTFE sheets. Two samples are taken for SAXS characterization: one of them before submitting the mixture to curing cycle (*in situ* SAXS analysis) and the other one

Table 1
Characteristics of components used

Vantico LY556, $\overline{M}_n = 382.6$ g mol^{-1}	Diglycidyl ether of bisphenol A (DGEBA) 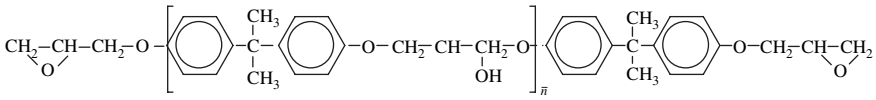
Aldrich, $M = 198$ g mol^{-1}	Methylene dianiline (MDA) 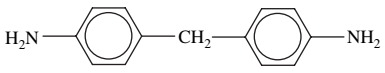
$\overline{M}_w = 89,847$ g mol^{-1}, $\overline{M}_n$ = Arkema = 43,431 g mol^{-1}, $\overline{M}_w/\overline{M}_n$ = 2069 Arkema	Poly(methylmethacrylate) (PMMA) 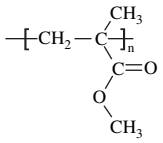

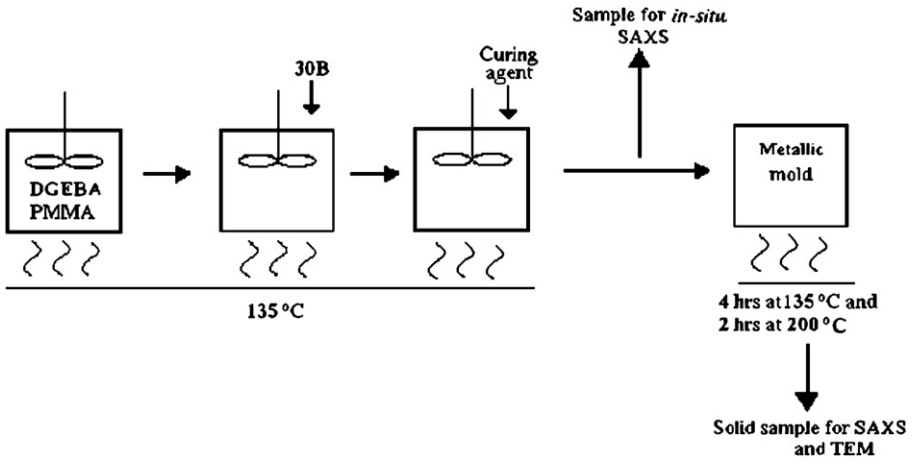

Fig. 2. Diagram of melt process used.

when the curing cycling is finished (SAXS analysis in the solid state). Designation of samples and preparation methodology are summarized in Table 2.

2.3. Characterization

Wide-angle-X-ray scattering (WAXS) was recorded by monitoring the 2θ diffraction angles from 1 to 10° on a SIEMENS D500 diffractometer with a Brentano Bragg geometry goniometer (40 kV, 30 mA, $\lambda = 1.54$ Å). Transmission electron microscopy (TEM) was performed on a Phillips CM 120 microscope operating at 80 kV. Phase separation was also checked using a Dynamic mechanical analysis (DMA), this was carried out on cured samples with a Rheometric Solid Analyser (RSAII) in order to obtain tensile dynamic mechanical spectra (storage modulus E', loss modulus E'' and loss factor $\tan\delta$) between 50 and 250 °C. Samples were parallelepipedic bars ($1.5 \times 2.5 \times 25$ mm^3). The small angle X-ray scattering (SAXS) apparatus is composed of a rotating X-ray source and a copper target ($\lambda = 1.542$ Å). The spectra were acquired for scattering vector q in the range 10^{-2} Å$^{-1} < q < 0.12$ Å^{-1}. Two dimensional SAXS patterns were recorded with a CCD Ropper Scientific detector. The 2D data were then circularly averaged to produce a one dimensional graph of scattering intensity $I(q)$ as a function of the wave vector, $q = 4\pi/\lambda \sin(\theta)$, where θ is the scattering angle. The scattered intensities were corrected for transmission, background and parasitic scattering. The *in situ* SAXS measurements were performed during the cure of the samples S_2 and S_4 at 135 °C, and for the cured samples S_1 and S_3 in the solid state at room temperature.

2.4. SAXS interpretation

Quantification of the structure associated with silicate layers is possible using small angle X-ray scattering (SAXS). A detailed discussion of the scattering theory of layers and plates can be found in Ref. [23]. The stacked-disc model has been used to explain the results obtained with small angle neutron and X-ray scattering [24]. Yet, the distribution of tactoid sizes is complex and these distributions as well as curvature contribute to the slope of the scattered intensity. These factors are not taken into account in this model. Furthermore, the stacked-disk model assumes a uniform distribution but neither the exfoliated platelets nor the tactoids present are uniformly dispersed throughout the matrix. As mentioned

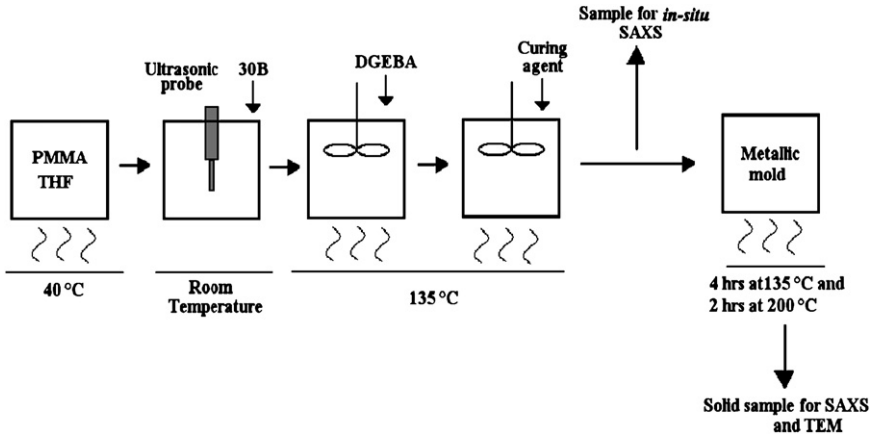

Fig. 3. Diagram of ultrasonic probe process used.

Table 2
Description and designation of studied nanocomposite blends

Sample	Signification and introduction way	Type of analysis
S_1	Ternary blend: ultrasonic probe technique; ([[PMMA + THF] + 30B] + DGEBA) + MDA: dispersion of clay in PMMA dissolved in THF with the ultrasonic probe for 1 h at room temperature; introduction of DGEBA within the mixture at 135 °C; dispersion by high speed for 2 h at 135 °C before adding the amine; curing cycle: 4 h at 135 °C and 2 h at 200 °C	TEM, WAXS, SAXS (on cured sample)
S_2	Ternary blend: ultrasonic probe technique; ([[PMMA + THF] + 30B] + DGEBA) + MDA: same process as S_1 and following up the curing during the isothermal step at 135 °C for 30 min for SAXS *in situ* studies	SAXS *in situ* at 135 °C during 30 min
S_3	Ternary blend: melt technique; [DGEBA + PMMA + 30B] + MDA: PMMA, clay, DGEBA are mixed for 2 h at 135 °C before adding the amine; curing cycle: 4 h at 135 °C and 2 h at 200 °C	TEM, WAXS, SAXS (on cured sample)
S_4	Ternary blend: melt technique; DGEBA + PMMA + 30B] + MDA: same process as S_3 and following up the curing during the isothermal step at 135 °C for 30 min for SAXS *in situ* studies	SAXS *in situ* at 135 °C during 30 min

by Hanley et al. [25] the use of this model is thus questionable, except for very low filler content. In this work, we have used the aspect ratio of a plate, and we have considered a wide distribution of tactoid thicknesses. In the case of flat particles of thickness, t, the small angle scattered intensity is given by the following law:

$$P(q) = \frac{B}{q^2}\Delta\rho^2 t^2 \left(\frac{\sin(qt/2)}{qt/2}\right)^2 \quad (1)$$

where B is a constant proportional to developed surface of the particles and $\Delta\rho$ is the difference of electronic densities of the matrix and of the filler [23]. A distribution of thicknesses was assumed and the spectrum was considered as being the sum of contributions of several populations, a fixed number of platelets in a stack constituting a population. The SAXS signal was thus fitted to the weighted sum of the contributions arising from entities of thickness t_i:

$$P(q) = \sum_{i=1}^{10} \frac{B_i}{q^2} t_i^2 \left(\frac{\sin(qt_i/2)}{qt_i/2}\right)^2 \quad (2)$$

A least square fitting procedure was applied to determine the parameters B_i and t_i. The proportion P_i of the tactoids of size t_i within the matrix was then estimated with the relation:

$$P_i = \frac{B_i}{\sum_j B_j}$$

Results from this methodology are in good agreement with the TEM results [26]. As already mentioned, the stacked-disc model does not take into account the interactions between different clay tactoids which may become more significant for greater clay loadings. In an attempt to account for the correlation bump originating from interparticle correlations observed in some of the nanocomposites in the high q range, the following structure factor was used:

$$S(q) = \frac{1}{1 + k\omega(q)} \quad (3)$$

$$\omega(q) = 3\frac{(\sin qd) - qd\cos(qd)}{(qd)^3} \quad (4)$$

where $\omega(q)$ is a form factor. Two new parameters are introduced: the characteristic distance d and k: d is thus a correlation length and can be seen as a pseudo spatial-periodicity, k describes the magnitude of correlation effects and can be considered as a pseudo order-factor [27]. The scattered intensity was then fitted to the product $P(q)S(q)$.

3. Main results and discussion

3.1. Morphology of cured PMMA epoxy blends

TEM characterization reported in Fig. 4 was made on sample containing 10 phr of PMMA and prepolymer cured with MDA hardener with a stoichiometric ratio under the same curing cycle as the samples with clay (4 h at 135 °C and 2 h at 200 °C). The objective was to detect and check the presence of the phase separation and identify the different morphologies. For this case, nodules of PMMA homogenously distributed within the thermoset matrix were obtained. The size of the nodules ranges between 30 and 70 nm. Fig. 5 presents the dynamic mechanical spectra of post cured blend containing 10 phr of PMMA. The phase separation is confirmed by the dynamic mechanical analysis which shows two relaxation peaks characteristics of thermoplastic and thermosets phase.

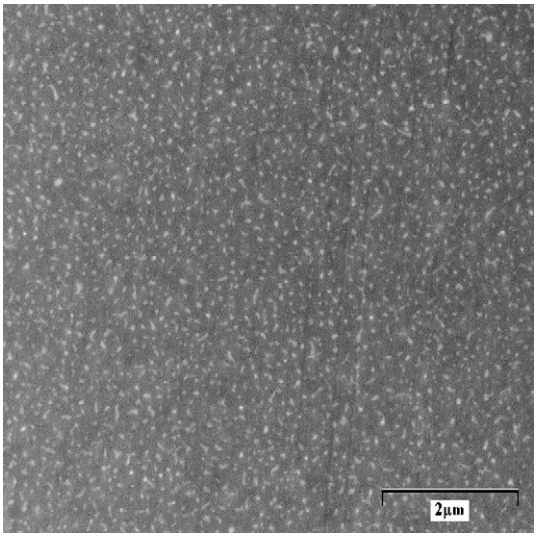

Fig. 4. Transmission electron micrograph obtained on DGEBA–MDA network with 10 phr PMMA.

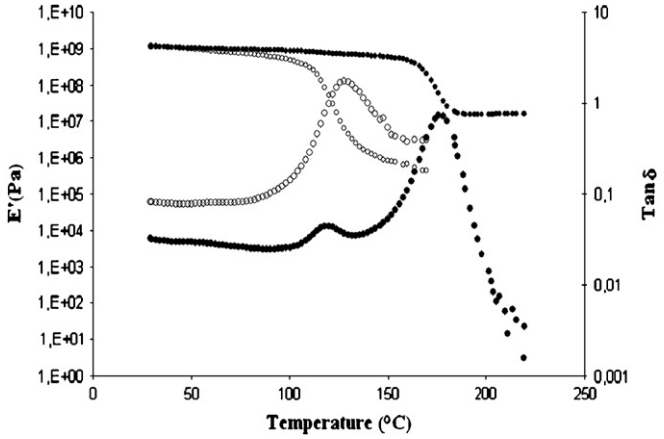

Fig. 5. Dynamic mechanical spectra (at a frequency of 1 Hz) for: (○) pure PMMA and (●) epoxy-amine blend with 10 phr PMMA.

The low temperature relaxation corresponds to the PMMA phase and the high temperature is linked to that of the epoxy phase relaxation.

3.2. Morphologies of cured PMMA epoxy nanocomposite blends

3.2.1. WAXS studies

Wide-angle-X-ray spectra performed on ternary blends obtained by ultrasonic probe (S_1) and by melt process (S_3), respectively, are presented in Fig. 6. Each spectrum is compared to pure Cloisite 30B, which shows clearly a well-defined peak at $2\theta = 5°$, assigned to the interlayer spacing $d_{001} = 1.79$ nm and characteristic of the clay crystalline structure. None of the nanocomposite spectra exhibits a diffraction peak which highlights the lack of repeated structures of equal spacings. As a result, dispersion in the WAXS window is at least achieved. But we cannot speak of exfoliation because the lack of Bragg scattering may only indicate that the distances between two consecutive platelets are too great to be detected (higher than 44 Å). We are only sure that monomers and increasing polymer chains have diffused into clay galleries and opened them.

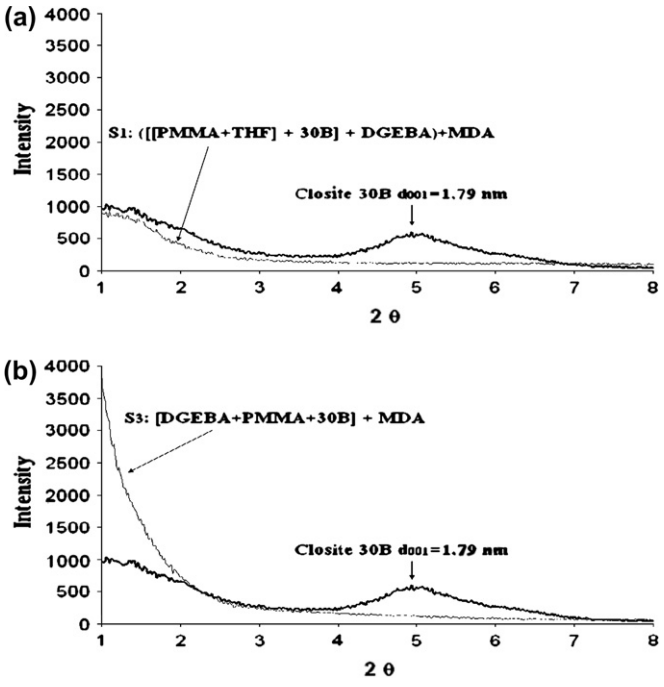

Fig. 6. X-ray diffraction patterns of the cured samples: (a) S_1, (b) S_3. Both of them are compared with the Cloisite 30B clay spectrum.

The X-ray spectrum performed on the ternary blends processed using the solvent technique (S_1) shows a different evolution in the small angle window, next to the direct beam. A correlation peak seems to appear unlike other nanocomposite. Further SAXS spectra window will clarify this point.

3.2.2. TEM studies

TEM is a method used to get a direct view of the dispersion state in all the materials. On the TEM micrograph, reported in Fig. 7a significant of the S_1 nanocomposite, the clay is homogeneously distributed and randomly dispersed throughout the matrix. Fig. 7b, obtained at higher magnification shows the presence of PMMA in the shape of small white nodules, resulting from the phase separation during curing of the epoxy-amine network [12]. The diameter of these particles ranges between 34 and 65 nm; the clay and the nodules are homogeneously distributed in the matrix. The TEM image at higher magnification reported in Fig. 7c shows that the tactoids present average interlayer distances of 22 nm.

To show the solvent and ultrasound probe effects on the morphology, TEM images performed on nanocomposites obtained without solvent were reported in Fig. 8. At low magnification (Fig. 8a) we observe the presence of small tactoids that coexist with large aggregates of silicate within the matrix. The distance of separation between them is about 10 μm and the size of the aggregates varies from 1 to 5 μm. In the same way at higher magnification (Fig. 8b), the small white nodules of PMMA form a separate phase with an average diameter of 70 nm.

At first sight, the use of solvent and ultrasonic probe is an efficient means to obtain a homogeneous dispersion of much smaller tactoids than the dispersion technique without solvent which leads to a considerable amount of clusters of much larger size. In both cases the phase separation is present. From these observations in both processes, it seems that clays are only contained in the epoxy continuous phase and are not observed inside PMMA nodules besides the presence of clay does not modify the phase separation of thermoplastic from the thermoset network. The TEM micrographs thus suggest that the best dispersion of small aggregates is obtained when the solvent and the ultrasonic probe are employed together. Yet, one must keep in mind that TEM is a local analytical technique and the distances measured on the micrographs are not really significant of the whole sample.

3.2.3. SAXS studies

As far as SAXS is concerned, two entities can give rise to diffusion: the platelets and the PMMA nodules (30–60 nm)

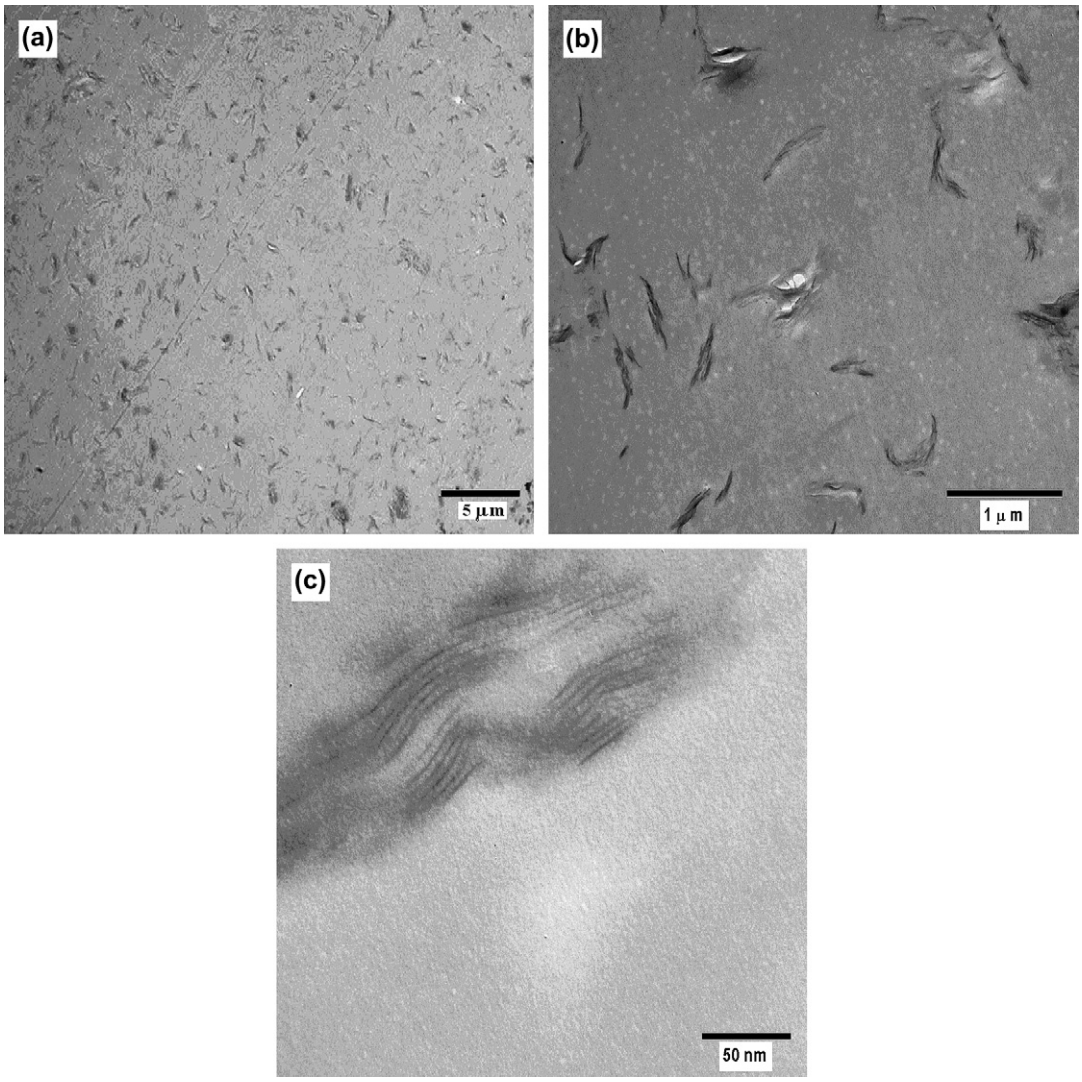

Fig. 7. TEM images of S_1 cured nanocomposite performed with solvent and an ultrasonic probe coupled with a high speed disperser (a) general view, (b) evidence of the phase separation due to PMMA, (c) separation of silicate monolayers.

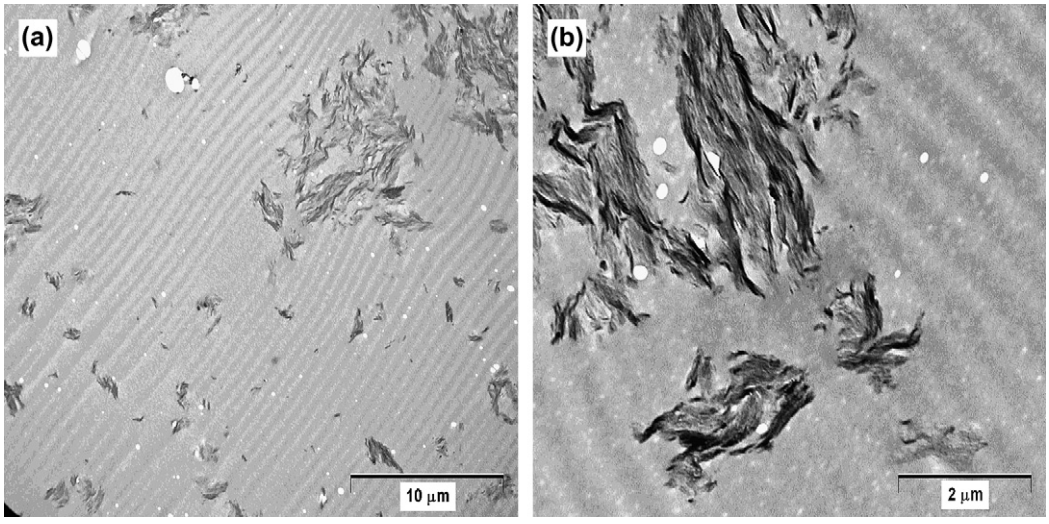

Fig. 8. TEM images of S_3 cured nanocomposite without solvent and performed with melt dispersion (a) view of the whole material, (b) evidence of the phase separation due to PMMA.

obtained during the phase separation. Yet, the contrast between the epoxy network and the PMMA particles is weak and the contribution of the PMMA nodules could not be observed in a sample without montmorillonite clay. The corresponding contribution to the scattered intensity is thus considered negligible compared to the diffusion by the platelets. The Lorentz corrected intensity profiles, Iq^2 *versus* q, in the nanocomposites S_1 and S_3 are displayed in Fig. 9a and b, respectively. The experimental data have been fitted by using Eq. (2) for S_3 nanocomposite and Eqs. (2)–(4) for S_1 nanocomposite.

In Fig. 9a and b, good agreement is obtained between the experimental profiles and the calculated intensities. The various populations of tactoid thickness obtained with a least square fitting procedure are summarized in Fig. 10 for the two samples S_1 and S_3.

On the SAXS pattern of S_1 ternary blend, the spectrum shows a correlation bump at $q_1 = 1.02\ \text{nm}^{-1}$ leading to an increase of the SAXS intensity at larger angles. This peak indicates a superstructure with a characteristic length equal to $d_1 = 2\pi/q_1 = 60$ Å. Its large width at half maximum shows that the characteristic length undergoes a lot of variations. This characteristic length can be considered as the average distance between two exfoliated platelets and confirms the WAXS data. This correlation bump is not observed on sample S_3, in this sample, TEM images have shown that the dispersion state is less uniform and that large aggregates coexist with exfoliated sheets and tactoids.

In the S_1 nanocomposite, a large population of diffusing entities with a thickness of 2 nm is observed. This population

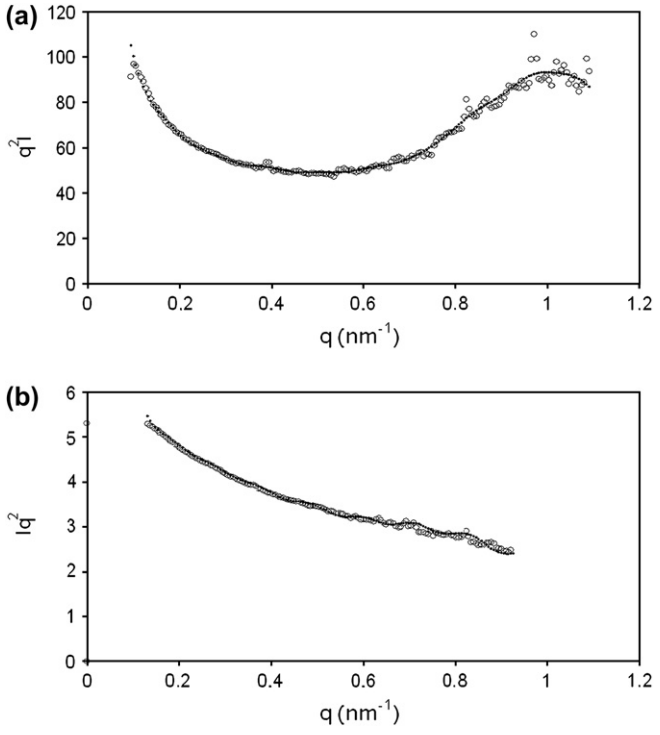

Fig. 9. SAXS spectra after Lorentz correction for (a) S_1 and (b) S_3 for: (○) the cured nanocomposites and (●) adjustment with Eq. (2).

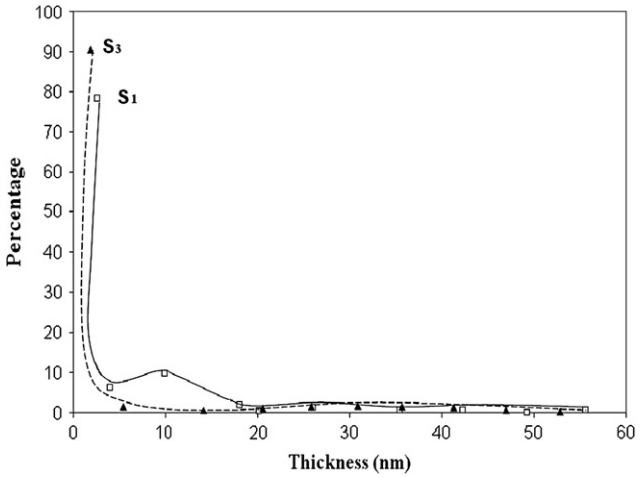

Fig. 10. Distributions of tactoid thickness in cured samples: (—□—) S_1 and (– – –▲– – –) S_3.

unambiguously corresponds stacks of one or two platelets. Nevertheless, tactoids of 10 nm containing 3–5 sheets are also present in the sample. In the S_3 nanocomposite, the proportion of particles with a thickness close to 2 nm is close to 80%. This nanocomposite seems to be the best exfoliated but due to the experimental uncertainties at very small angles, only entities smaller than 50–100 nm can be observed by SAXS. Thus the proportion of micron-size agglomerates has not been taken into account, especially in the sample S_3.

It is interesting to note that the scattered intensity profile in the S_1 nanocomposite can be fitted on the whole scattering vector range with Eqs. (2)–(4) with a good accuracy. The distributions of populations obtained are very similar to the one obtained on the basis of Eq. (2) in the low q range. The fitting parameter obtained is $d = 62$ Å, in good agreement with the characteristic distance d obtained with the Bragg relation.

These three analysis techniques are really complementary because they cover several observation scales. Transmission electron microscopy, extended from several micrometers to tens of nanometers, shows that the more homogeneous and the finest dispersion is obtained when the solvent and the ultrasonic probe are used together. But the SAXS results (from a few nanometers up to 100 nm) conclude the opposite because the proportion of micron-size agglomerates observed by TEM on samples processed without solvent cannot be detected by SAXS since only entities smaller than 100 nm can be measured. As a result, when the observation scale is still decreased, the exfoliation of platelets is much more obvious in the WAXS measurement window (from a few angstroms up to tens of angstroms).

3.3. Following in situ of the exfoliation process

3.3.1. SAXS studies

In order to have additional information on the dispersion state of the platelets during the curing reaction, the exfoliation process has been followed *in situ* with SAXS measurements. The evolution of the Lorentz corrected SAXS intensity profile

as a function of the reaction time is given in Fig. 11a and b for S_2 and S_4, respectively.

The SAXS spectral changes can be understood if one keeps in mind that the exfoliating particles have a decreasing size, which corresponds to an increasing scattering vector. Moreover, these particles may be out of the q range investigated and may not be detected if they are too large or too small. No correlation bump can be observed on the spectrum of S_4 nanocomposite (Fig. 11b), whereas very different behaviour is obtained in Fig. 11a which is associated with sample S_2. For the S_2 nanocomposite, the evolution of the SAXS spectra can be understood as follows. At the beginning of the reaction, large size agglomerates corresponding to very low q values ($q < 0.1$ nm^{-1}) are exfoliated and this process leads to an increase of the scattered intensity for q around 0.1 nm^{-1}, which is the lower limit of the q range investigated. For longer reaction times, the exfoliation goes further and the intensity rises for increasing q values. In the final state, a correlation bump appears for scattering vectors close to 1 nm^{-1} as already mentioned in the study of the cured state. The Lorentz corrected intensity decreases less rapidly around $q = 0.1$ nm^{-1} for increasing reaction time. This evolution can be associated to the decrease of the thicknesses of the diffusing entities. The distribution of the thicknesses of the diffusing entities and

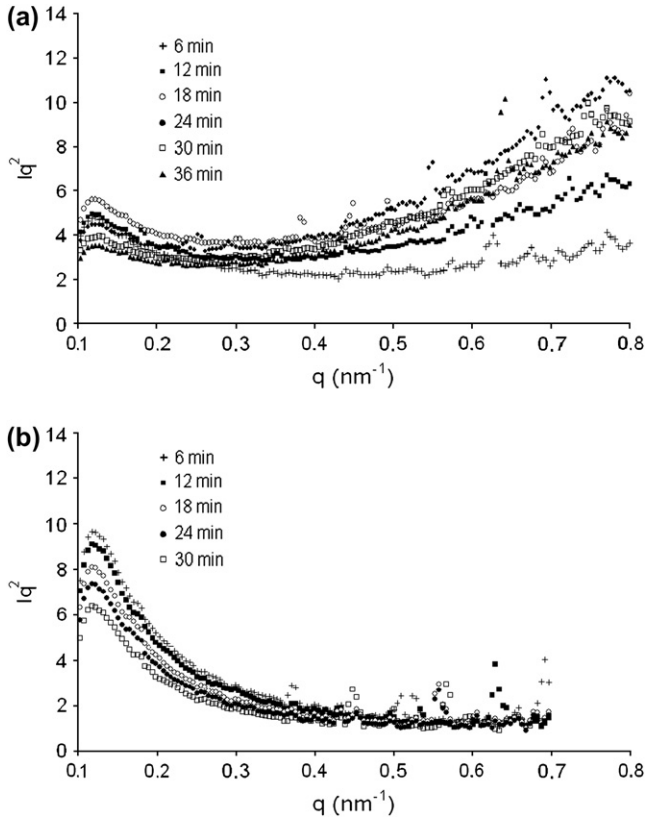

Fig. 11. SAXS profiles performed on the (a) S_2 nanocomposite obtained during the curing process at 135 °C for various reaction times: (+) $t = 6$ min, (■) $t = 12$ min, (○) $t = 18$ min, (●) $t = 24$ min, (□) $t = 30$ min, (▲) $t = 36$ min; (b) S_4 nanocomposite obtained during the curing process at 135 °C for various reaction times: (+) $t = 6$ min, (■) $t = 12$ min, (○) $t = 18$ min, (●) $t = 24$ min, (□) $t = 30$ min.

their evolution with the reaction time could be obtained from the fitting of the experimental data with Eqs. (2) and (4). These evolutions are summarized in Fig. 12a and b.

In Fig. 12a, for the S_2 sample at $t = 6$ min, a population of tactoids of 5 nm is obtained and several populations of particles are present between 20 and 60 nm with low proportions. The 5 nm thickness populations correspond to quasi exfoliated particles of 2 or 3 sheets. At $t = 12$ min, a bimodal population of particles with a thickness close to 5 and 20 nm is observed. The 5 nm thick populations correspond to exfoliated clay particles. The 20 nm size tactoids are likely to originate from large size aggregates which have been destroyed. They were out of the q range and size range investigated at $t = 6$ min and could not be detected. The amount of the various populations of different sizes seems to change rather arbitrarily as a function of time but this can be attributed to these populations entering the SAXS range successively. At $t = 18$ min, the two former populations are changed in population of thicknesses 2 and 8 nm, respectively. At $t = 24$ min, the proportion of 10 nm large particles decreases and the population of exfoliated sheets increases. At $t = 30$ min, this exfoliation process goes further.

For longer reaction times, the 2 nm thickness population of exfoliated clays increases. After $t = 36$ min, the exfoliation process can be considered as complete, no change in the SAXS profile can be observed and the proportion of the various tactoids is similar to the one obtained for the cured sample S_2 considered in Fig. 10. At the end of the curing cycle, only exfoliated clays are detected. Yet, large agglomerates of more than 60 nm may still be present in the nanocomposite and cannot be detected in the SAXS window.

In Fig. 12b, for the S_4 nanocomposite, a similar exfoliation process can be followed. A wide distribution of tactoid thickness is obtained at $t = 6$ min, with a maximum in the range 10–20 nm. For $t = 12$ min, a population of about 8 nm thickness diffusing entities is present. This population corresponds to stacks of two or three layers, resulting from the de-aggregation of the 10–20 nm thick agglomerates obtained for $t = 6$ min. The thickness of theses entities decreases with increasing reaction time. For $t = 18$ min, a population of 4–5 nm thick diffusing entities is observed. Then for $t = 24$ min, an exfoliated microstructure appears in the nanocomposite with isolated particles showing a thickness close to 2 nm [24,25]. At $t = 30$ min, the proportion of individual exfoliated sheets is similar to the one previously measured on the cured S_3 sample.

In the S_2 and S_4 nanocomposites, SAXS experiments showed that the large tactoids exfoliated and form particles with different numbers of platelets. In the S_2 nanocomposite, a population of large size tactoids has to be considered to take into account the results. This population is destroyed and the resulting tactoids enter the range of thicknesses investigated. At the end of the reaction, homogeneously distributed platelets lead to a correlation bump. In the S_4 nanocomposites, the exfoliation process is not so complete and homogeneous. It is likely that large size agglomerates are still present in the sample, as suggested by the TEM observations. In both

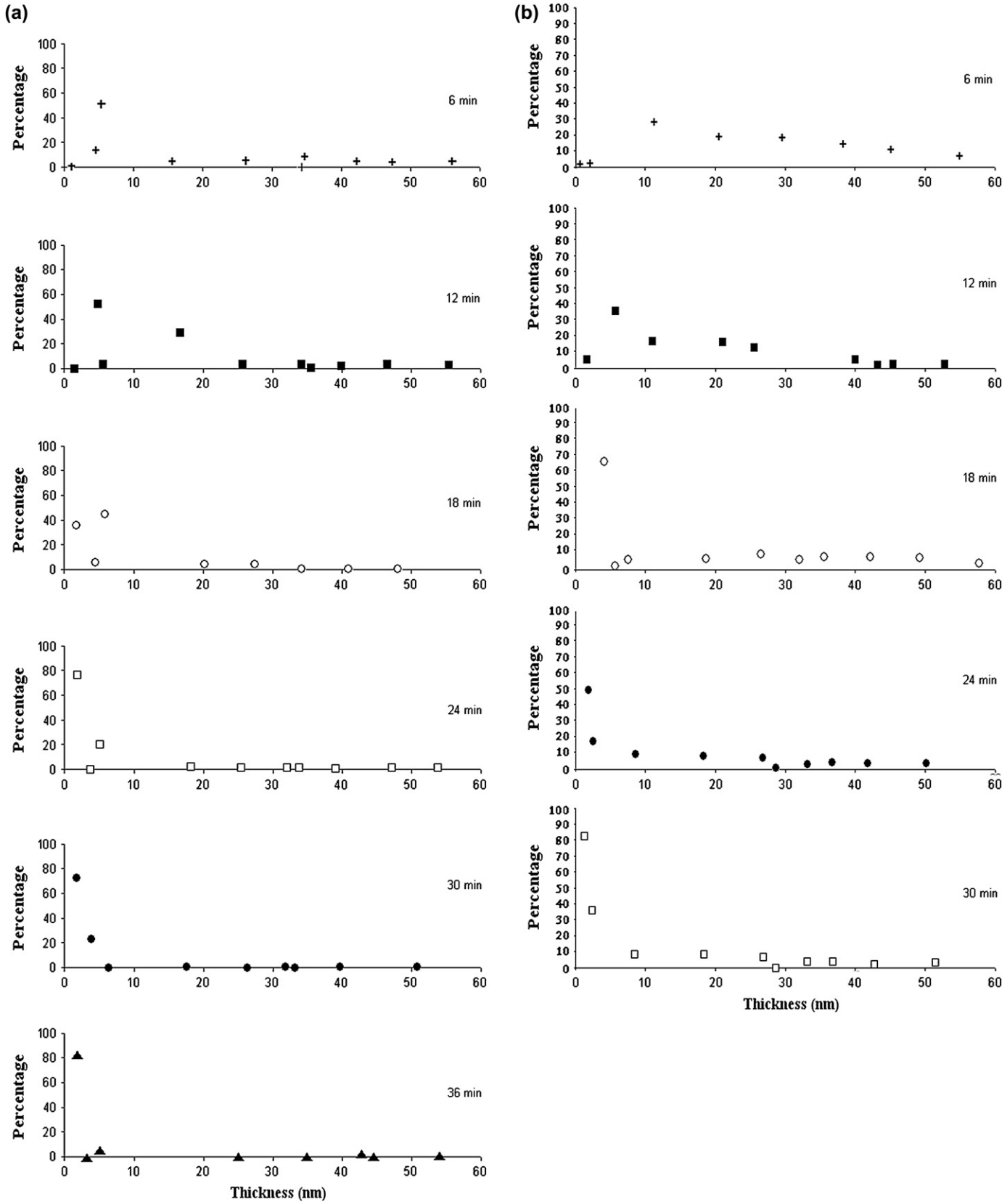

Fig. 12. Distribution of tactoid thickness calculated on (a) S_2 sample as a function of time (+) $t = 6$ min, (■) $t = 12$ min, (○) $t = 18$ min, (●) $t = 24$ min, (□) $t = 30$ min, (▲) $t = 36$ min; (b) S_4 sample as a function of time (+) $t = 6$ min, (■) $t = 12$ min, (○) $t = 18$ min, (●) $t = 24$ min, (□) $t = 30$ min.

samples, several populations of particles have to be considered in the nanocomposites: exfoliated platelets, tactoids of a few platelets and micrometer size tactoids. Tactoids are the basic unit of the morphology which exists in the form of micron or larger domains with varying concentration or orientation.

It is important and interesting to point out that some platelets move into the matrix after the gel time in these nanocomposites. The gel time for these systems is about 15 min at 135 °C and the scattering spectra change until $t = 30$ min and $t = 36$ min for the samples S_2 and S_4, respectively. The highest mobility is obtained in the S_2 samples, around q range, $q = 1\ \mathrm{nm}^{-1}$, corresponding to the smaller length scales investigated in our SAXS measurements. Traditionally, some authors have proposed that after the gel time, the crosslinked structure between the epoxy and the hardener blocked the movement of the clay tactoids [28]. At this point, it is important to say that in these studies no SAXS characterization was developed, the analysis by WAXS was the only evidence for giving a total exfoliation time. The SAXS results of the present work suggest that sometimes it is possible to obtain a weak movement (not detectable by WAXS) of tactoids even after the macroscopic gel point.

The mechanisms of clay exfoliation can help us to give an explanation. Under fast curing conditions, the cured epoxy chains have not enough time to allow stress relaxation and as a result, they store much more elastic energy than chains polymerized under slow curing conditions. The elastic forces work for clay layer separation, whereas the sum of viscous forces, attractive forces arising due to electrostatic attraction and the Van der Waals forces work against the exfoliation. If elastic forces are higher than the sum of the other forces, exfoliation of clays takes place [11]. The temperature and the amine used in this work are parameters that can be considered as fast curing conditions, the elastic forces are still present even when the gel point has been reached and they were put into evidence indirectly by the movement of the clay detected by SAXS.

4. Conclusions

1. Epoxy–clay–PMMA ternary systems were obtained by two independent techniques of mixing: melt and ultrasonic probe dispersion, respectively. In both cases, phase separation of polymer PMMA was obtained like nodular morphology with a regular distribution within the epoxy-amine matrix. Besides, with both dispersion techniques clay particles were dispersed into the scale of tactoids, these were more homogenously distributed when the ultrasonic probe dispersion was employed since tactoids of 10 nm containing 3–5 sheets are present in the samples, whereas for the melt technique large size agglomerates are observed. The nodular morphology surrounds the clay dispersed like tactoids and there is no evidence that the PMMA phase could enter into the galleries.
2. SAXS analysis gives an insight into the mechanism of dispersion and into the relative efficiency of the systems of dispersion used. It was shown that with the same materials but employing different mechanisms of initial dispersion, the exfoliation process can significantly differ.
3. Exfoliation state of the silicate layers in blends synthesised by both techniques has been investigated on the cured systems and during the curing reaction. The attention was focussed on the distribution of thicknesses of the diffusing particles. SAXS analysis has shown that exfoliation of the platelets can occur through the de-aggregation of large agglomerates into particles composed of a few platelets. At the end of the process, the filler is well dispersed as single sheets. SAXS *in situ* study made on samples obtained by ultrasonic probe dispersion, shows that final morphology is more homogeneously exfoliated, and correlations cannot be neglected between the exfoliated sheets, whereas that for sample got by melt dispersion, large size agglomerates are present with single platelets and no correlation peak is observed. This technique has shown also that movements at the scale of nanometers of clay tactoids could be possible even after the gel point.

Studies are in progress dealing with the nature and the molecular weight of the PMMA.

Mechanical and barrier properties of these ternary nanocomposites will be investigated in the near future.

Acknowledgement

The authors would like to thank CONACYT (México) for the grant to Marcelo Hernandez. The authors thank Pierre Alcouffe for providing the TEM characterization and Ruben Vera for performing the XRD experiments.

References

[1] Alexandre M, Dubois P. Mater Sci Eng 2000;R28(1–2):1–63.
[2] Pinnavaia TJ, Beall GW. Polymer–clay nanocomposite. New York: Wiley; 2001.
[3] Usuki A, Kojima Y, Kawasumi M, Okada A, Fukushima Y, Kurauchi T, et al. J Mater Res 1993;8(5):1179–84.
[4] Lan T, Kaviratna PD, Pinnavaia TJ. Chem Mater 1995;7(11):2144–50.
[5] Kormann X, Lindberg H, Berglund L. Polymer 2001;42(10):4493–9.
[6] Kormann X, Thomann R, Mulhaupt R, Finter J, Berglund L. J Appl Polym Sci 2002;86(10):2643–52.
[7] Le Pluart L, Duchet J, Sautereau H. Polymer 2005;46(26):12267–78.
[8] Zeng QH, Yu AB, Lu M, Paul DR. J Nanosci Nanotechnol 2005;5(10): 1574–92.
[9] Le Pluart L, Duchet J, Sautereau H, Halley P, Gerard J-F. Appl Clay Sci 2004;25(3–4):207–19.
[10] Pascault J, Sautereau H, Verdu J, William RJJ. Thermosetting polymers. New York: Marcel Dekker; 2002.
[11] Park JH, Jana SC. Polymer 2003;44(7):2091–100.
[12] Ritzenthaler S, Girard-Reydet E, Pascault JP. Polymer 2000;41(16): 6375–86.
[13] Gomez CM, Bucknall CB. Polymer 1993;34(10):2111–7.
[14] Vinneta N, Setua D, Mathur GN, Kamal KK. J Appl Polym Sci 2004; 93(5):2201–10.
[15] Vermogen A, Boucard S, Duchet J, Masenelli-Varlot K, Prele P, Seguela R. Macromolecules 2005;38(23):9661–9.

[16] Lincoln DM, Vaia RA, Wang GZ, Hsiao BS. Polymer 2001;42(4): 1621–31.
[17] Lincoln DM, Vaia RA, Wang GZ, Hsiao BS, Krishnamoorti R. Polymer 2001;42(25):9975–85.
[18] Chen C, Curlis D. Nanotechnology 2003;14(6):643–8.
[19] Yoonessi M, Toghiani H, Daulton TL, Lin JS, Pittman CU. Macromolecules 2005;38(3):818–31.
[20] Varlot K, Reynaud E, Kloppfer MH, Vigier G, Varlet J. J Polym Sci Part B Polym Phys 2001;39(12):1360–70.
[21] Kong D, Park CE. Chem Mater 2003;15(2):419–24.
[22] Lam C, Lau K, Cheung H, Ling H. Mater Lett 2005;59(11):1369–72.
[23] Porod G. General theory in small angle X-ray scattering. London: Academic Press; 1982.
[24] Hanley HJM, Muzny DD, Butler BD. Langmuir 1997;13(20):5276–82.
[25] Hanley HJM, Muzny DD, Ho DL, Glinka CJ. Langmuir 1997;19(14): 5575–80.
[26] Varlot K, Reynaud E, Vigier G, Varlet J. J Polym Sci Part B Polym Phys 2002;40(3):272–83.
[27] Hajji P, David L, Gerard JF, Pascault JP, Vigier G. J Polym Sci Part B Polym Phys 1999;37(22):3172–87.
[28] Lü J, Ke Y, Qi Z, Yi X-S. J Polym Sci Part B Polym Phys 2001; 39(1):115–20.